JCTC Journal of Chemical Theory and Computation

Article

Cite This: J. Chem. Theory Comput. 2018, 14, 2558−2569

pubs.acs.org/JCTC

Recovering Intrinsic Fragmental Vibrations Using the Generalized Subsystem Vibrational Analysis

Yunwen Tao,[†] Chuan Tian,[‡] Niraj Verma,[†] Wenli Zou,[§] Chao Wang,[∥] Dieter Cremer,[⊥,†] and Elfi Kraka*[,†]

[†]Department of Chemistry, Southern Methodist University, 3215 Daniel Avenue, Dallas, Texas 75275-0314, United States

[‡]Department of Chemistry, Stony Brook University, Stony Brook, New York 11794, United States

[§]Institute of Modern Physics, Northwest University, Xi'an, Shaanxi 710127, P. R. China

[∥]Institute of Nuclear Energy Safety Technology, Chinese Academy of Sciences, Hefei, Anhui 230031, P. R. China

ABSTRACT: Normal vibrational modes are generally delocalized over the molecular system, which makes it difficult to assign certain vibrations to specific fragments or functional groups. We introduce a new approach, the Generalized Subsystem Vibrational Analysis (GSVA), to extract the intrinsic fragmental vibrations of any fragment/subsystem from the whole system via the evaluation of the corresponding effective Hessian matrix. The retention of the curvature information with regard to the potential energy surface for the effective Hessian matrix endows our approach with a concrete physical basis and enables the normal vibrational modes of different molecular systems to be legitimately comparable. Furthermore, the intrinsic fragmental vibrations act as a new link between the Konkoli−Cremer local vibrational modes and the normal vibrational modes.

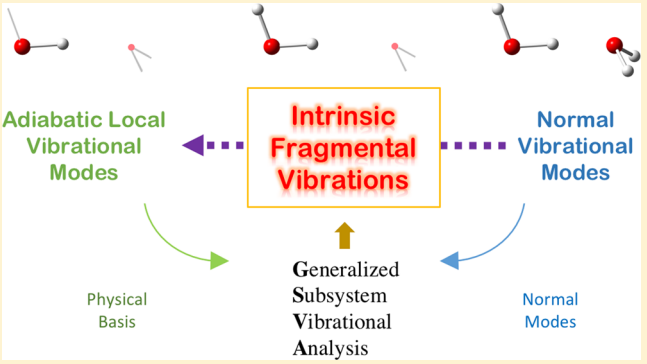

1. INTRODUCTION

Vibrational spectroscopy is a powerful tool for structure elucidation. Raman and infrared (IR) spectroscopy can be used not only for the assignment of characteristic peaks to identify functional groups but also to characterize the electronic structure of the targeted chemical system. With the rapid development of quantum chemical methods based on quantum mechanics (QM), the simulation of vibrational spectra has been made feasible and becomes a complementary tool in structural determination. The vibrational frequencies of any chemical species can be calculated from the normal mode analysis (NMA) by solving the Wilson equation of vibrational spectroscopy.[1]

However, normal modes extend over the whole molecule, which complicates the analysis and interpretation of vibrations for large polyatomic molecules and molecules in solution or other media being described by a multiscale model, i.e., QM/MM. For example, in the water dimer, if one wants to compare the normal vibrational modes of either the H-bond donor water or the acceptor water with the vibrations of a single water molecule in gas phase in order to characterize the influence of hydrogen bonding, one has to consider that the normal mode vectors in the two systems are of different lengths (18 versus 9).

Obtaining normal modes being projected into a targeted subsystem or fragment would be the natural way to solve the above problem and allow the normal modes to be intrinsically comparable among different molecular systems.

Many efforts have been made in this direction. Head proposed a strategy to calculate the vibrations for adsorbates on surfaces by diagonalizing the partial Hessian for atoms of adsorbates.[2] His contribution fostered the work of Li and Jensen, who developed the partial Hessian vibrational analysis (PHVA) method,[3] where a subblock of the Hessian matrix is diagonalized and all atoms except the subsystem are assigned an infinitely large atomic mass. This approach has been applied by Besley and co-workers to calculate C═O stretching and C−H stretching vibrations in organic molecules.[4,5] Ghysels and co-workers proposed the mobile block Hessian (MBH) approach as an extension to PHVA in order to calculate "localized" normal vibrational modes for partially optimized molecular systems.[6−10] The MBH method allows one to calculate the vibrations of a subsystem which has been fully optimized, while the remaining parts of the system are treated as rigid bodies being allowed to translate and rotate. Thus, the computational costs can be reduced because one does not need to calculate the full Hessian matrix of the whole system. The MBH method has been implemented in quantum chemical packages including ADF and Q-Chem. Woodcock and co-workers developed another method called vibrational subsystem analysis (VSA),[11] partitioning a large system into a subsystem and its environment. The vibrational modes led by the subsystem are

Received: November 18, 2017
Published: April 10, 2018

DOI: 10.1021/acs.jctc.7b01171
J. Chem. Theory Comput. 2018, 14, 2558−2569

calculated, and the environment follows the motions of the subsystem in an adiabatic way. However, we need to note that VSA was initially developed to couple the global motion to a local subsystem in a large molecule, e.g., protein, in order to estimate the free energy contribution from subsystems. Zheng and cowork applied VSA to obtain approximate low-frequency normal modes of proteins for conformational sampling.[12] VSA was also used in another work for mapping the full Hessian matrix onto a coarse-grained scale for macromolecules.[13] A review article by Ghysels and co-workers compares the PHVA, MBH, and VSA methods.[14] Jacob and Reiher developed a special approach to localize normal modes contributing to certain bands with the help of a defined criterion.[15] Their method is tailored to polypeptides and proteins. Recently, Huix-Rotllant and co-worker provided a procedure to localize normal modes of fragment(s) by taking the submatrices of the full Hessian as local Hessian matrices.[16] The advantage of this approach is that besides diagonalizing the local Hessian matrices, the corresponding eigenvectors are used for the transformation of the full Hessian. Thus, the information on the full Hessian can be utilized.

However, if one tries to apply the methods mentioned above in order to obtain intrinsically comparable normal vibrations of a subsystem, the following problems must be resolved:

- As shown in Figure 1, all methods involve the direct partitioning of the full Hessian matrix into the red sub-block for the targeted subsystem or fragment and another blue sub-block for the remaining part as its environment. Once the Hessian matrix is partitioned, the information describing the interaction between the subsystem and the environment contained in the green sub-block is damaged or even eliminated. This casts doubt on the usefulness of these localized normal modes.
- The so-called "local Hessian matrix" or its counterpart with different names pertinent to the subsystem is not in a proper form prepared for characterizing the normal vibrational modes of the subsystem. If the total number of translations and rotations for the subsystem is k, then such a local Hessian matrix is expected to have and only have k eigenvalues of zero.
- As normal modes are delocalized over the whole system, any attempt to compare the vibrational frequencies of the localized subsystem modes with the frequencies of the normal modes of the whole system either from *ab initio* calculations or measured vibrational spectra is not appropriate. This implies that verifying the results of the localized normal modes with the help of vibrational frequencies calculated from the full Hessian is problematic. A more reasonable approach for result validation is thus desired.
- Some methods were tested against selected examples containing many C−H, N−H, and C═O bonds. The stretching modes of these bonds are in nature localized to these fragments, and they can contribute to more significant infrared intensities than other types of vibrational motions due to large dipole changes. This will give the illusion that the localized normal modes have been accurately determined.
- Some approaches partition the complete system according to certain rules, e.g., containing the peptide bond unit in the subsystem. However, a generally applicable approach is expected to allow arbitrary partitioning of the whole system into the subsystem and its environment.
- The purpose of localizing of normal vibrational modes should be re-evaluated. While theoretical chemists have developed various kinds of localized properties or models including localized orbitals,[17−21] localized atomic charges,[22−27] and even localized electron densities[28,29] in order for simplification, comparison, and analysis, we expect that localized normal modes should be able to serve for similar tasks instead of assisting the assignment of the absorption peaks from vibrational spectra for different functional groups.

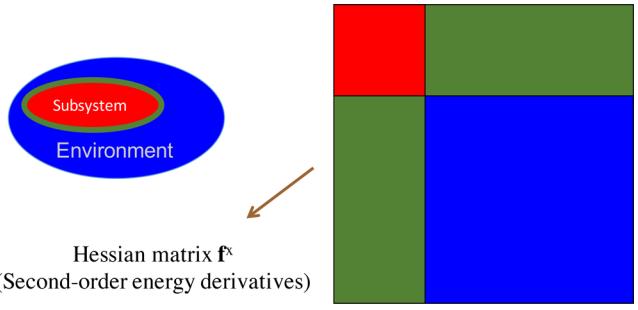

Figure 1. Schematic diagram of partitioning of the Hessian matrix.

We start from a different ansatz in order to obtain intrinsically comparable normal vibrations of a subsystem or fragment. When calculating the normal modes of any chemical system, three ingredients are required by the Wilson equation: Cartesian coordinates **R**, atomic masses **M**, and the Hessian matrix in Cartesian coordinates $\mathbf{f}^x$. As long as this system is at a stationary point on the potential energy surface with all three ingredients available, the Wilson equation can be solved accordingly. If one is interested in obtaining the normal vibrational modes for a subsystem/fragment, it is obvious that the Cartesian coordinates **R** and atomic masses **M** of this part should stay the same. The problem to be solved is then how to obtain the "effective Hessian matrix" that is reasonable and physically sound for the subsystem. Only on this basis, the resulting localized normal vibrational modes of the subsystem can be then obtained from solving the Wilson equation of vibrational spectroscopy using the effective Hessian matrix.

In this work, we introduce a new approach called Generalized Subsystem Vibrational Analysis (GSVA) that is based on a physically solid "effective Hessian matrix" which preserves the information on the curvature of the potential energy surface for the subsystem/fragment as it is in the whole system with a full Hessian matrix. The normal vibrational modes calculated by this approach are therefore called "intrinsic fragmental vibrations". These vibrations are not constructed from an arbitrary model, instead they are recovered specifically for the subsystem from the full Hessian matrix. Noteworthy is that a distinction should be made between the GSVA method introduced in this work and the VSA method[11] developed by Woodcock. This paper is structured in the following way: The theory of the GSVA is derived and described first. After summarizing the Computational Details section, in the Results and Discussion section, six different examples for calculating the intrinsic fragmental vibrations of their subsystems are discussed. The conclusions, along with some notes of applying and implementing GSVA, are given in the last section.

DOI: 10.1021/acs.jctc.7b01171
J. Chem. Theory Comput. 2018, 14, 2558−2569

2. METHODOLOGY

The normal vibrational modes of a molecular system can be calculated from the solution of the Wilson equation of vibrational spectroscopy[1] based on the Hessian matrix $\mathbf{f}^x$ in Cartesian coordinates collecting the second-order derivatives of the energy with regard to the displacement of atomic nuclei. The dimension of $\mathbf{f}^x$ is $3N \times 3N$, where N is the number of atoms in the system.

As the translation and rotation of the system render no change to the potential energy, matrix $\mathbf{f}^x$ is singular and has K zero eigenvalues, K takes the value of 5 for linear molecules or 6 for nonlinear molecules. We are, in general, only interested in the nonzero eigenvalues λ_μ (collected in the diagonal matrix $\mathbf{\Lambda}$) as well as their eigenvectors $\mathbf{c}_\mu$ (collected in matrix $\mathbf{C}$), as shown in eq 1. The dimensions of $\mathbf{C}$ and $\mathbf{\Lambda}$ are $3N \times (3N - K)$ and $(3N - K) \times (3N - K)$, respectively.

$$\mathbf{f}^x\mathbf{C} = \mathbf{C}\mathbf{\Lambda} \tag{1}$$

As each eigenvector $\mathbf{c}_\mu$ in $\mathbf{C}$ is orthonormalized, $\mathbf{C}^T\mathbf{C} = \mathbf{I}_{3N-K}$, eq 1 can be rewritten into

$$\mathbf{C}^T\mathbf{f}^x\mathbf{C} = \mathbf{\Lambda} \tag{2}$$

and

$$\mathbf{C}\mathbf{C}^T\mathbf{f}^x\mathbf{C}\mathbf{C}^T = \mathbf{C}\mathbf{\Lambda}\mathbf{C}^T = \mathbf{f}^x \tag{3}$$

We define a new matrix $\mathbf{Q} = \mathbf{C}\mathbf{C}^T$. As $\mathbf{Q}^2 = \mathbf{C}\mathbf{C}^T\mathbf{C}\mathbf{C}^T = \mathbf{C}\mathbf{I}\mathbf{C}^T = \mathbf{C}\mathbf{C}^T = \mathbf{Q}$, $\mathbf{Q}$ is thus a projection matrix in the dimension of $3N \times 3N$. An interesting equation results as follows:

$$\mathbf{Q}\mathbf{f}^x\mathbf{Q} = \mathbf{f}^x \tag{4}$$

The $3N - K$ eigenvectors collected in matrix $\mathbf{C}$ span the full internal vibration space; thus, when projection operator $\mathbf{Q}$ multiplies $\mathbf{f}^x$ from the left to the right of $\mathbf{f}^x$, $\mathbf{f}^x$ is not changed.

This special property of the Hessian matrix $\mathbf{f}^x$ can be extended to any other projection matrix, as long as this projection matrix can span the full internal vibration space. We choose to use the internal coordinates to span the same space, as translations and rotations can be simply excluded.

For a molecule system being composed of N atoms, we can use $3N - K$ internal coordinates to specify its geometry. The internal coordinates are related to the Cartesian coordinates via the Wilson B matrix[1]

$$\mathbf{B} = \frac{\partial \mathbf{q}}{\partial \mathbf{x}} \tag{5}$$

where $\mathbf{x}$ are the Cartesian coordinates and $\mathbf{q}$ are the internal coordinates. For the above nonredundant set of $3N - K$ internal coordinates, the corresponding Wilson B matrix $\mathbf{B}$ has the dimension of $(3N - K) \times 3N$. As matrix $\mathbf{B}$ is rectangular, its Moore–Penrose inverse matrix $\mathbf{B}^+$ is calculated by

$$\mathbf{B}^+ = \mathbf{B}^T(\mathbf{B}\mathbf{B}^T)^{-1} \tag{6}$$

so that

$$\mathbf{B}\mathbf{B}^+ = \mathbf{I}_{3N-K} \tag{7}$$

where the trace of the identity matrix $\mathbf{I}_{3N-K}$ as $3N - K$.

We define a matrix $\mathbf{A}$

$$\mathbf{A} = \mathbf{B}^+\mathbf{B} \tag{8}$$

as $\mathbf{A}^2 = \mathbf{B}^+\mathbf{B}\mathbf{B}^+\mathbf{B} = \mathbf{B}^+\mathbf{I}\mathbf{B} = \mathbf{B}^+\mathbf{B} = \mathbf{A}$; matrix $\mathbf{A}$ is also a projection matrix having the similar properties as matrix $\mathbf{Q}$ in eq 4, leading to the following equations:

$$\mathbf{f}^x = \mathbf{A}\mathbf{f}^x\mathbf{A} \tag{9}$$

$$\mathbf{f}^x = (\mathbf{B}^+\mathbf{B})\mathbf{f}^x(\mathbf{B}^+\mathbf{B}) \tag{10}$$

According to the properties of pseudoinverse $\mathbf{B}^+$, we have

$$(\mathbf{B}^+\mathbf{B})^T = \mathbf{B}^+\mathbf{B} \tag{11}$$

Equation 10 can be rewritten into

$$\mathbf{f}^x = (\mathbf{B}^+\mathbf{B})^T\mathbf{f}^x(\mathbf{B}^+\mathbf{B}) \tag{12}$$

$$\mathbf{f}^x = \mathbf{B}^T(\mathbf{B}^+)^T\mathbf{f}^x\mathbf{B}^+\mathbf{B} \tag{13}$$

$$\mathbf{f}^x = \mathbf{B}^T(\mathbf{B}^T)^+\mathbf{f}^x\mathbf{B}^+\mathbf{B} \tag{14}$$

then

$$\mathbf{f}^x = \mathbf{B}^T(\mathbf{B}(\mathbf{f}^x)^+\mathbf{B}^T)^{-1}\mathbf{B} \tag{15}$$

Noteworthy is that eq 15 is a more general form of the equations for $\mathbf{f}^x$ above. Furthermore, this equation offers an opportunity to obtain the effective Hessian matrix for a fragment or subsystem within the whole system.

Suppose that within the molecular system with N atoms, a subsystem has n atoms ($n < N$). The geometry of this subsystem can be specified by $3n - k$ internal coordinates (k = 5 or 6 depending on whether its geometry is linear or nonlinear). The Wilson B matrix for these $3n - k$ internal coordinates in the complete system can be calculated as $\mathbf{B}'$ with the dimension of $(3n - k) \times 3N$. In the subsystem, the corresponding Wilson B matrix for the same set of internal coordinates is calculated as $\mathbf{B}'_{sub}$ with the dimension of $(3n - k) \times 3n$. In order to simplify the analysis, we rearrange the labels of n atoms of the subsystem within the whole system, so that the first n atoms denote the subsystem. It is obvious that matrix $\mathbf{B}'_{sub}$ corresponds to the first $3n$ columns of matrix $\mathbf{B}'$, while the elements of the rest $3(N - n)$ columns in $\mathbf{B}'$ are simply zero. We define an effective Hessian matrix $\mathbf{f}^x_{sub}$ for the subsystem with the help of eq 15

$$\mathbf{f}^x_{sub} = \mathbf{B}'^T_{sub}(\mathbf{B}'(\mathbf{f}^x)^+\mathbf{B}'^T)^{-1}\mathbf{B}'_{sub} \tag{16}$$

where $(\mathbf{f}^x)^+$ is the Moore–Penrose inverse of $\mathbf{f}^x$. Here, $\mathbf{f}^x_{sub}$ is a symmetric matrix in the dimension of $3n \times 3n$, and more importantly, it has exactly k zero eigenvalues.

However, we need to note that eqs 9, 10, and 12–14 cannot be used for this purpose, namely

$$\mathbf{f}^x_{sub} \neq (\mathbf{B}'^+\mathbf{B}'_{sub})^T\mathbf{f}^x(\mathbf{B}'^+\mathbf{B}'_{sub}) \tag{17}$$

because the Wilson B matrix and related pseudoinverse in these equations can no longer span the full vibration space for the whole system, only for the subsystem.

The effective Hessian matrix $\mathbf{f}^x_{sub}$ for the subsystem can be directly used for normal mode analysis by solving the Wilson equation of vibrational spectroscopy given its Cartesian coordinates and atomic masses as it can be done for the whole system based on full Hessian matrix $\mathbf{f}^x$. Noteworthy is that in the process of obtaining $\mathbf{f}^x_{sub}$ no partitioning/sub-blocking of the original Hessian matrix $\mathbf{f}^x$ is introduced. Instead, the full Hessian matrix $\mathbf{f}^x$ is projected into the unique internal vibrational space of the subsystem in eq 16, which strikingly differentiates our approach from others.[2,3,6,15,16]

DOI: 10.1021/acs.jctc.7b01171
J. Chem. Theory Comput. 2018, 14, 2558–2569

Furthermore, it is necessary to evaluate the physical basis and correctness of the effective Hessian matrix derived in this work, if intrinsically comparable normal vibrations are desired on the basis of such an effective Hessian matrix. The seemingly most straightforward approach to validate our model is to compare the normal mode frequencies of the subsystem based on effective Hessian matrix $\mathbf{f}^x_{sub}$ and those based on the original Hessian matrix $\mathbf{f}^x$ for the whole system. However, one needs to be careful that normal modes are delocalized over the system in question, and it is not appropriate to compare the normal modes within the subsystem and those modes beyond it.[30] In this work, we choose to calculate and compare the local vibrational modes[31−35] proposed by Konkoli and Cremer for $\mathbf{f}^x_{sub}$ and $\mathbf{f}^x$ because these local modes have been proved as the only and unique local equivalents of normal vibrational modes in terms of internal coordinates[30] which can be directly compared among different molecular systems, and they have been used to quantify the intrinsic strength of chemical bonding[36−42] as well as to characterize the local properties of the electronic structure.[43,44] The characterization of local vibrational modes including related local mode force constants and local mode frequencies is called local mode analysis. For each local vibrational mode driven by a specific internal coordinate as the "leading parameter", we can calculate the corresponding local force constant or its synonym as adiabatic force constant k^a_n as well as the local vibrational frequency ω^a_n. These two quantities can be related with the help of the Wilson G matrix[1,45]

$$(\omega^a_n)^2 = \frac{1}{4\pi^2 c^2} k^a_n G_{nn} \tag{18}$$

For the purpose of validating the effective Hessian matrix, calculating the local force constants k^a_n is sufficient.

In this work, we take a simplified form[30,46] of calculating the adiabatic force constant k^a_n by

$$\frac{1}{k^a_n} = \mathbf{b}(\mathbf{f}^x)^+\mathbf{b}^T \tag{19}$$

where $\mathbf{f}^x$ is the Hessian matrix for the whole system in Cartesian coordinates, and its Moore−Penrose inverse is denoted as $(\mathbf{f}^x)^+$. Row vector $\mathbf{b}$ is the Wilson B matrix for an internal coordinate parameter q_n (e.g., bond stretching, angle bending, dihedral torsion, etc.) within the subsystem leading this local mode. Here, $\mathbf{b}$ is in the dimension of $1 \times 3N$.

Based on the effective Hessian matrix $\mathbf{f}^x_{sub}$ of the subsystem, its adiabatic force constant $k^a_{n,sub}$ of the local mode led by the same internal coordinate q_n is calculated by

$$\frac{1}{k^a_{n,\mathrm{sub}}} = \mathbf{b}_{sub}(\mathbf{f}^x_{sub})^+\mathbf{b}^T_{sub} \tag{20}$$

where $\mathbf{b}_{sub}$ is the first $3n$ elements of $\mathbf{b}$ in eq 19, and $(\mathbf{f}^x_{sub})^+$ is the Moore−Penrose inverse of $\mathbf{f}^x_{sub}$. Equation 20 can be expanded by substituting $\mathbf{f}^x_{sub}$ using eq 16

$$\frac{1}{k^a_{n,\mathrm{sub}}} = \mathbf{b}_{sub}(\mathbf{B}'^T_{sub}(\mathbf{B}'(\mathbf{f}^x)^+\mathbf{B}'^T)^{-1}\mathbf{B}'_{sub})^+\mathbf{b}^T_{sub} \tag{21}$$

According to the properties of the pseudoinverse, eq 21 can be rewritten as

$$\frac{1}{k^a_{n,\mathrm{sub}}} = \mathbf{b}_{sub}\mathbf{B}'^+_{sub}(\mathbf{B}'^T_{sub}(\mathbf{B}'(\mathbf{f}^x)^+\mathbf{B}'^T)^{-1})^+\mathbf{b}^T_{sub} \tag{22}$$

$$\frac{1}{k^a_{n,\mathrm{sub}}} = \mathbf{b}_{sub}\mathbf{B}'^+_{sub}\mathbf{B}'(\mathbf{f}^x)^+\mathbf{B}'^T(\mathbf{B}'^T_{sub})^+\mathbf{b}^T_{sub} \tag{23}$$

$$\frac{1}{k^a_{n,\mathrm{sub}}} = \mathbf{b}_{sub}\mathbf{B}'^+_{sub}\mathbf{B}'(\mathbf{f}^x)^+\mathbf{B}'^T(\mathbf{B}'^+_{sub})^T\mathbf{b}^T_{sub} \tag{24}$$

then

$$\frac{1}{k^a_{n,\mathrm{sub}}} = (\mathbf{b}_{sub}\mathbf{B}'^+_{sub}\mathbf{B}')(\mathbf{f}^x)^+(\mathbf{b}_{sub}\mathbf{B}'^+_{sub}\mathbf{B}')^T \tag{25}$$

The calculation of the matrix product of $\mathbf{b}_{sub}\mathbf{B}'^+_{sub}\mathbf{B}'$ is visualized by the Falk diagram shown in Figure 2.

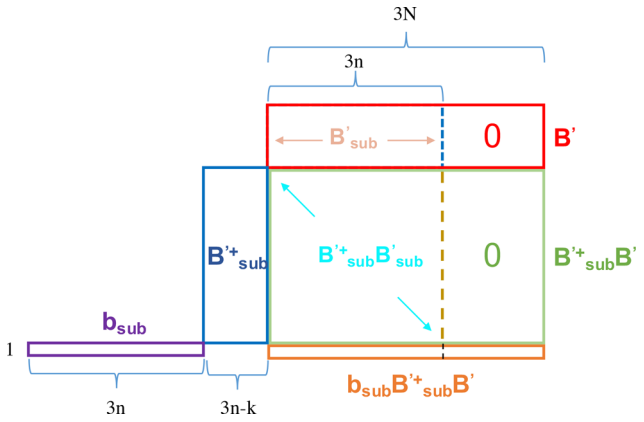

Figure 2. Falk diagram of matrix multiplication for $\mathbf{b}_{sub}\mathbf{B}'^+_{sub}\mathbf{B}'$.

In matrix $\mathbf{B}'$, the block of the first $3n$ columns is matrix $\mathbf{B}'_{sub}$, while the elements in the remaining $3(N - n)$ columns are zeros. The multiplication of $\mathbf{B}'^+_{sub}$ with $\mathbf{B}'$ leads to a projection matrix $\mathbf{B}'^+_{sub}\mathbf{B}'_{sub}$ in the first $3n$ columns of $\mathbf{B}'^+_{sub}\mathbf{B}'$ and zeros in the remaining $3(N - n)$ columns.

As the Wilson B matrix $\mathbf{B}'_{sub}$ (or $\mathbf{B}'$) collects the nonredundant set of $3n - k$ internal coordinate parameters describing the geometry of the subsystem, the projection matrix $\mathbf{B}'^+_{sub}\mathbf{B}'_{sub}$ spans the complete internal coordinate space and also the internal vibration space of the subsystem. The Wilson B matrix row vector $\mathbf{b}_{sub}$ for any internal coordinate parameter (no matter whether it is included in the set of the $3n - k$ parameters or not) in the subsystem can be expressed as a linear combination of $3n - k$ row vectors in $\mathbf{B}'_{sub}$. So we get

$$\mathbf{b}_{sub}\mathbf{B}'^+_{sub}\mathbf{B}'_{sub} = \mathbf{b}_{sub} \tag{26}$$

which constitutes the first $3n$ elements of the row vector $\mathbf{b}_{sub}\mathbf{B}'^+_{sub}\mathbf{B}'$, and the rest of the $3(N - n)$ elements are zeros. Also, we have

$$\mathbf{b}_{sub}\mathbf{B}'^+_{sub}\mathbf{B}' = \mathbf{b} \tag{27}$$

where $\mathbf{b}$ is from eq 19. Then, eq 25 can be simplified as

$$\frac{1}{k^a_{n,\mathrm{sub}}} = \mathbf{b}(\mathbf{f}^x)^+\mathbf{b}^T \tag{28}$$

Also interesting is that

$$k^a_{n,\mathrm{sub}} = k^a_n \tag{29}$$

which means the local mode analysis with regard to any internal coordinate in the subsystem based on the effective Hessian matrix $\mathbf{f}^x_{sub}$ is equivalent to the local mode analysis for the same internal coordinate based on the full Hessian matrix $\mathbf{f}^x$.

DOI: 10.1021/acs.jctc.7b01171
J. Chem. Theory Comput. 2018, 14, 2558−2569

Furthermore, as the adiabatic force constant k_n^a characterizes the curvature of the Born−Oppenheimer potential energy surface (PES) given in a specific direction defined by the internal coordinate as the leading parameter,[41] the curvature of the PES driven by any one of the internal coordinates in the subsystem within the whole system is retained in the effective Hessian matrix. In other words, the standalone subsystem with effective Hessian matrix "feels" exactly the same curvature of the PES with regard to the internal local vibrations as it is within the whole system based on the full Hessian matrix. In this way, the underlying physical nature of the vibrations of the subsystem calculated based on $\mathbf{f}_{sub}^x$ is kept invariant, and this gives our approach the capability and advantage to characterize the intrinsically comparable normal vibrations of subsystems or fragments in any molecular system. We call these intrinsically comparable normal vibrations the intrinsic fragmental vibrations.

3. COMPUTATIONAL DETAILS

In this work, all *ab initio* calculations including geometry optimization and Hessian evaluation were performed using the Gaussian 09 package.[47] The dimers, trimers, and monomers of water and ammonia molecules were calculated at the ωB97X-D/6-311++G(d,p) level;[48−51] The hydrogen disulfide molecule and the hydrogen disulfide-water cluster were calculated at the B3LYP/6-31G(d,p) level of theory;[52−55] The methane molecule and methane-C_{60} complex were calculated using the Minnesota hybrid functional M06-2X with Pople's 6-31G(d,p) basis set.[56] Grimme's empirical D3 dispersion correction was added to the nuclear repulsion force.[57] The formaldehyde molecule and formaldehyde-nanotube complex were calculated at the B3LYP/6-31G(d,p) level with Grimme's empirical D3 dispersion correction with Becke−Johnson (BJ) damping.[58] The propane molecule along with a reference methane molecule were calculated with Hartree−Fock theory[59] using 6-31G(d,p) basis set. For the above density functional theory (DFT) calculations, the UltraFine integration grid was used, and all systems were optimized to local minima with tight convergence criteria.

The calculations of the effective Hessian matrices, local mode analysis, and normal mode analysis were carried out with the program package COLOGNE2017.[60]

4. RESULTS AND DISCUSSION

In the following section, we discuss the results of the intrinsic fragmental vibrations in six different molecular systems. For each subsystem or fragment having n atoms, we calculated its $3n - k$ intrinsic fragmental vibrational frequencies based on the effective Hessian matrix $\mathbf{f}_{sub}^x$ in the dimension of $3n \times 3n$.

Then, we calculated the frequencies of normal vibrational modes or intrinsic fragmental vibrations of the same subsystem in the gas phase or other chemical systems, respectively, for all six examples in order to demonstrate that the intrinsic fragmental vibrations have the advantage of being directly compared and analyzed laterally among different systems.

We have also calculated the local mode force constants of the leading internal coordinate parameters q_n within the fragment/subsystem based on both the full Hessian $\mathbf{f}^x$ and the effective Hessian $\mathbf{f}_{sub}^x$ in order to verify the physical relevance of these intrinsic fragmental normal vibrations.

4.1. Water Dimer $(H_2O)_2$. The first example is the water dimer which has a hydrogen bond between two water molecules, one serving as the H-bond donor and the other as the H-bond acceptor (Figure 3). One water molecule has three

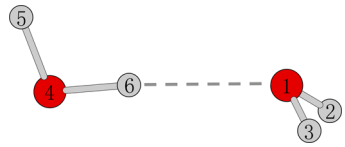

Figure 3. Water dimer structure in C_s symmetry. Red balls represent oxygen atoms, and gray balls represent hydrogen atoms.

normal vibrational modes, including the H−O−H angle bending, symmetric O−H stretching, and asymmetric O−H stretching with increasing vibrational frequencies (Table 1).

Table 1. Comparison of Normal Mode Frequencies of Water Monomers

No.	Donor[a] (cm^{-1})	Acceptor[a] (cm^{-1})	H_2O[b] (cm^{-1})
1	1531	1607	1609
2	3775	3891	3903
3	3976	3997	4012

[a]Columns "Donor" and "Acceptor" denote the intrinsic fragmental vibrational frequencies of donor and acceptor water molecules based on their effective Hessian matrices, respectively. [b]Column "H_2O" collects the normal mode frequencies of a water molecule in gas phase as the reference.

The introduction of another water molecule in a dimer structure brings in an addition nine vibrational modes. These nine vibrational modes include the three internal vibrations of the second water molecule, three relative rotations, and three relative translations between these two water molecules. However, these nine new vibrations will mix with each other. Furthermore, the original three vibrations of the first water molecule are also mixed in, which potentially hinders the analysis of normal vibrational modes of either water molecule in the dimer.

Within the framework of GSVA, the donor/acceptor water is taken as a subsystem. Its effective Hessian matrix $\mathbf{f}_{sub}^x$ can be extracted by choosing a nonredundant set of three internal coordinate parameters according to eq 16. In a water molecule, we can choose two O−H distances and the H−O−H angle as a complete nonredundant parameter set. Therefore, matrix $\mathbf{B}'$ takes the dimension of 3×18, while matrix $\mathbf{B}'_{sub}$ is in the 3×9 dimension. Or we can use two O−H distances and the H−H distance to construct another parameter set, although the H−H distance does not imply H−H bonding in a water molecule. These two sets of parameters give two identical effective Hessian matrices, which reveals the flexibility and robustness of the GSVA approach; namely, this approach does not depend on the choice of the nonredundant internal parameter set. As long as the chosen set of parameters can unambiguously specify the geometry of the subsystem, GSVA will work.

Table 1 lists the three normal vibrational frequencies calculated by solving the Wilson equation[1] based on the effective Hessian matrices for the donor and acceptor waters. The resulting three normal modes calculated by GSVA are the unique counterparts of the normal modes of the water molecule in the gas phase. Correlating the intrinsic fragmental vibrational modes with those of the water molecule in the gas phase leads to the normal vibrational frequency ordering shown in Table 1. The acceptor water shows smaller deviations from the reference

DOI: 10.1021/acs.jctc.7b01171
J. Chem. Theory Comput. 2018, 14, 2558−2569

frequencies compared to the donor water. In the acceptor water, the first normal mode dominated by the H−O−H angle bending has the deviation of only 2 cm^{-1}, while the donor water's deviation is 78 cm^{-1}. This can be explained by the fact that the angle bending mode of the acceptor water is not affected by the formation of a hydrogen bond, while the angle bending of the donor water is hindered by this hydrogen bond. The larger deviations for the symmetric and asymmetric O−H stretching modes for the donor water are also caused by the hydrogen bonding which weakens the donor O−H covalent bond.[40,42]

For the purpose of validating the intrinsic fragmental vibrational modes and their frequencies, we calculated the local mode force constants of the O−H bond stretching and H−O−H angle bending modes in the donor and acceptor waters based on the effective Hessian matrix and the full Hessian matrix using eqs 19 and 20. The comparison of the local mode force constants in Table 2 shows that the values of $k^a_{n,sub}$ and k^a_n for local mode parameters within the subsystem are the same.

Table 2. Comparison of Local Mode Force Constants Based on Effective Hessian Matrix $\mathbf{f}^x_{sub}$ and Full Hessian Matrix $\mathbf{f}^x$ for Water Molecules

No.[a]	q_n[b]	$k^a_{n,sub}$	k^a_n
D-1	R(4−5)	8.691	8.691
D-2	R(4−6)	7.984	7.984
D-3	α(5−4−6)	0.596	0.596
A-1	R(1−2)	8.624	8.624
A-2	R(1−3)	8.624	8.624
A-3	α(2−1−3)	0.652	0.652

[a]In the "No." column, "D" denotes donor water, while "A" denotes acceptor water. [b]For internal coordinate q_n, parameter "R" stands for bond stretching. Unit for local mode force constant is mdyn/Å, while "α" is for angle bending and corresponding unit for local mode force constant is mdyn×Å/rad^2.

This clearly reveals that the effective Hessian matrices $\mathbf{f}^x_{sub}$ calculated for the donor/acceptor water molecules have retained the curvature of the PES of the whole system with regard to any internal coordinate in donor or acceptor water, respectively. Accordingly, these fragmental vibrational modes based on $\mathbf{f}^x_{sub}$ are thus intrinsic.

4.2. Ammonia Trimer $(NH_3)_3$. The ammonia trimer ring shown in Figure 4 has C_{3h} symmetry. All three ammonia molecules connected via hydrogen bonds are identical with regard to geometry as well as electronic structure. In this example, we want to take one ammonia molecule as the subsystem and obtain its intrinsic fragmental vibrations.

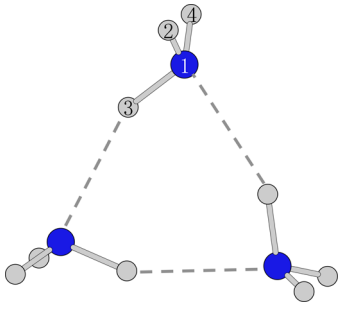

Figure 4. Ammonia trimer ring structure with C_{3h} symmetry. Blue balls represent nitrogen atoms, and gray balls represent hydrogen atoms.

For each ammonia molecule having four atoms, we need six internal coordinates to determine its geometry. The set of three N−H bonds and three H−N−H angles is the easiest option. But we can also use three N−H bonds and three H−H distances as a valid set for GSVA. Therefore, matrix $\mathbf{B}'$ has the dimension of 6 × 36, and matrix $\mathbf{B}'_{sub}$ has the dimension of 6 × 12.

Table 3 lists the intrinsic fragmental vibrational frequencies of ammonia in comparison with the normal mode frequencies of an ammonia molecule in the gas phase. While the symmetry of ammonia in the gas phase is reduced from C_{3v} to C_s for the ammonia in the trimer system shown in Figure 4, normal modes Nos. 2−3 and Nos. 5−6 lose their 2-fold degeneracy leading to the splitting in the vibrational frequency values. We find vibrations Nos. 2 and 4 of ammonia in the trimer have their frequency differences larger than 100 cm^{-1} when compared with the reference ammonia in the gas phase. Normal mode No. 2 is dominated by the rocking of the H3 atom, and normal mode No. 4 is basically the symmetric stretching of all three N−H bonds. As bond N1−H3 directly participates in the hydrogen bonding, the above two vibrational modes will be affected accordingly. However, the smallest difference in the vibrational frequency is found for No. 6 as 13 cm^{-1}. This vibration mode is dominated by the asymmetric stretching of bonds N1−H2 and N1−H4, which are not directly involved in hydrogen bonding.

Table 3. Comparison of Normal Mode Frequencies of Ammonia Monomers

No.	NH_3 in trimer (cm^{-1})	NH_3 in gas phase (cm^{-1})
1	1044	1003
2	1544	1672
3	1648	1672
4	3410	3523
5	3588	3658
6	3645	3658

The verification of the results from GSVA is carried out in Table 4.

4.3. Hydrogen Disulfide in a Water Cluster. Besides the small molecular clusters of water and ammonia, we built a cluster of hydrogen disulfide surrounded by 22 water molecules to simulate the solvation of hydrogen disulfide in liquid water (Figure 5). In this example, we want to calculate the intrinsic fragmental vibrations of the hydrogen disulfide molecule.

Table 4. Comparison of Local Mode Force Constants Based on Effective Hessian Matrix $\mathbf{f}^x_{sub}$ and Full Hessian Matrix $\mathbf{f}^x$ for Ammonia Molecule

No.	q_n[a]	$k^a_{n,sub}$	k^a_n
1	R(1−3)	6.480	6.480
2	R(1−2)	7.056	7.056
3	R(1−4)	7.056	7.056
4	α(2−1−4)	0.606	0.606
5	α(2−1−3)	0.541	0.541
6	α(3−1−4)	0.541	0.541

[a]Parameter "R" stands for bond stretching, while "α" is for angle bending. Unit of local mode force constant for bond stretchings and angles is mdyn/Å and mdyn×Å/rad^2, respectively.

DOI: 10.1021/acs.jctc.7b01171
J. Chem. Theory Comput. 2018, 14, 2558−2569

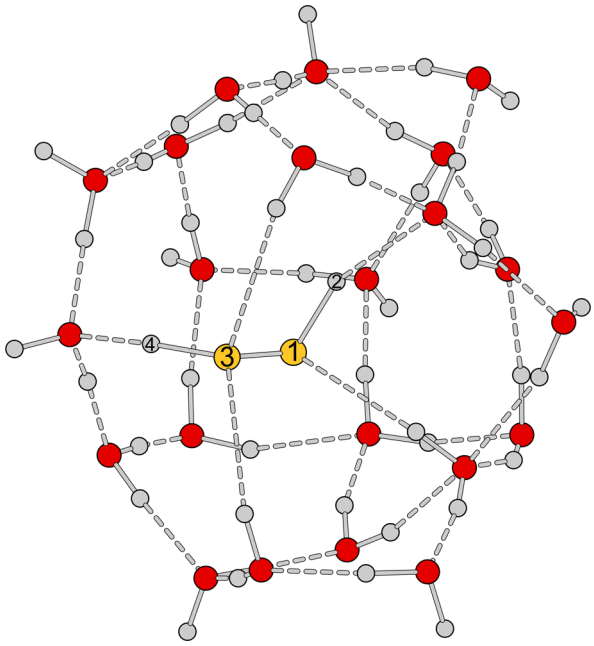

Figure 5. Structure of the hydrogen disulfide molecule in a water cluster of $(H_2O)_{22}$. Yellow balls are sulfur atoms, red are oxygens, and gray are hydrogens. Dashed lines represent noncovalent interactions, i.e., hydrogen bonds.

As for a complete nonredundant set of internal coordinate parameters required by GSVA, we choose two S−H bonds, the S−S bond, two S−S−H angles, and the H−S−S−H dihedral angle to obtain the effective Hessian matrix $\mathbf{f}^x_{sub}$ for the H_2S_2 molecule as the subsystem. These six internal coordinates construct corresponding matrices $\mathbf{B}'$ and $\mathbf{B}'_{sub}$ in the dimensions of 6 × 210 and 6 × 12, respectively.

The fragmental vibrations of the H_2S_2 molecule in the cluster calculated by GSVA (Table 5) show a shift of at least 30 cm^{-1}

Table 5. Comparison of Normal Mode Frequencies of Hydrogen Disulfide Molecule

No.	H_2S_2 in water cluster (cm^{-1})	H_2S_2 in gas phase (cm^{-1})
1	383	434
2	500	495
3	861	894
4	936	895
5	2452	2637
6	2355	2639

with regard to the reference H_2S_2 in the gas phase. Vibrations Nos. 5 and 6 have the largest deviations, and they are dominated by the S3−H4 and S1−H2 bond stretching, respectively. As these two S−H bonds donate S−H···OH_2 hydrogen bonds to surrounding water molecules, they are weakened in their bond strength leading to corresponding red shifts. However, vibration No. 2 has only a shift of 5 cm^{-1}. This vibration is dominated by the S−S bond stretching, which is hardly affected by the surrounding water molecules.

The local mode force constants of H_2S_2 within the cluster were calculated based on both the effective Hessian $\mathbf{f}^x_{sub}$ and the full Hessian $\mathbf{f}^x$ as shown in Table 6.

4.4. Methane (CH_4) in C_{60}. The methane-intercalated C_{60} structure was synthesized by Kwei and co-workers in 1997[61] (Figure 6). While the fullerene molecule has I_h symmetry and

Table 6. Comparison of Local Mode Force Constants Based on Effective Hessian Matrix $\mathbf{f}^x_{sub}$ and Full Hessian Matrix $\mathbf{f}^x$ for Hydrogen Disulfide Molecule

No.	$q_n{}^a$	$k^a_{n,sub}$	k^a_n
1	R(1−2)	3.332	3.332
2	R(1−3)	2.172	2.172
3	R(3−4)	3.197	3.197
4	α(2−1−3)	0.809	0.809
5	α(4−3−1)	0.790	0.790
6	τ(2−1−3−4)	0.082	0.082

[a]Parameter "R" stands for bond stretching, "α" is for angle bending, and "τ" is for dihedral torsion. Unit of local mode force constant for bond stretchings and angles is mdyn/Å and mdyn×Å/rad^2, respectively.

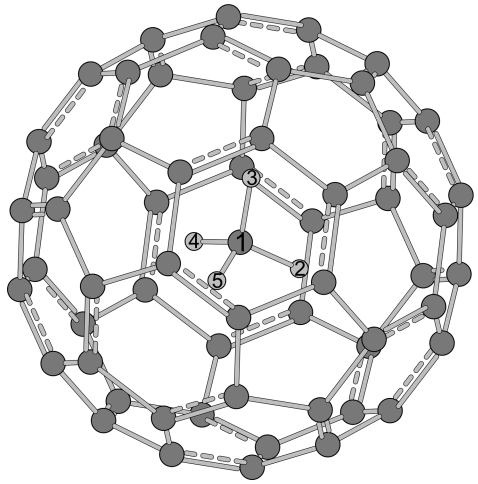

Figure 6. Structure of methane encapsulated in fullerene (C_{60}). Large balls represent carbon atoms, and small balls represent hydrogens.

methane has T_d symmetry, the complex has T symmetry. However, the methane encapsulated within the C_{60} molecule has still the T_d symmetry. It would be of interest to obtain the intrinsic fragmental vibrations of the methane inside the C_{60} in order to characterize this encapsulation effect.

As a complete nonredundant set of internal coordinates for the methane molecule, four C−H bonds and five H−C−H angles were chosen, although in total six H−C−H angles are available. Therefore, corresponding matrices of $\mathbf{B}'$ and $\mathbf{B}'_{sub}$ have the dimensions of 9 × 195 and 9 × 15, respectively.

In Table 7, the fragmental vibrational frequencies of methane within C_{60} calculated by GSVA are compared with normal mode frequencies of methane in the gas phase. All 2-fold and 3-fold degeneracies are kept as a result of the retention of T_d symmetry. The largest deviation is found for vibration No. 6 as a blue shift of 70 cm^{-1}. This vibration is dominated by the symmetric stretching of the four C−H bonds, which is largely affected by the C_{60} cage.

Table 8 lists the local mode force constants of the methane molecule in C_{60} calculated based on both the effective Hessian $\mathbf{f}^x_{sub}$ and the full Hessian $\mathbf{f}^x$. The data in Table 8 reveals that these two sets of local mode force constants are identical. Besides the nine parameters (Nos. 1−9) we used to obtain $\mathbf{f}^x_{sub}$, we have also calculated the local mode force constant of the sixth angle which was not included in the parameter set, and we obtained the same value as for the other five angles. This clearly shows that the local mode analysis can still work for the internal

DOI: 10.1021/acs.jctc.7b01171
J. Chem. Theory Comput. 2018, 14, 2558−2569

Table 7. Comparison of Normal Mode Frequencies of Methane Molecule

No.	CH_4 in C_{60} (cm^{-1})	CH_4 in gas phase (cm^{-1})
1	1328	1356
2	1328	1356
3	1328	1356
4	1583	1584
5	1583	1584
6	3150	3080
7	3250	3205
8	3250	3205
9	3250	3205

Table 8. Comparison of Local Mode Force Constants Based on Effective Hessian Matrix $\mathbf{f}^x_{sub}$ and Full Hessian Matrix $\mathbf{f}^x$ for Methane Molecule

No.[a]	q_n[b]	$k^a_{n,sub}$	k^a_n
1	R(1−2)	5.675	5.675
2	R(1−3)	5.675	5.675
3	R(1−4)	5.675	5.675
4	R(1−5)	5.675	5.675
5	α(2−1−3)	0.647	0.647
6	α(2−1−4)	0.647	0.647
7	α(2−1−5)	0.647	0.647
8	α(3−1−4)	0.647	0.647
9	α(3−1−5)	0.647	0.647
10*	α(4−1−5)	0.647	0.647

[a]Parameter labeled with * indicates this internal coordinate is not used as part of the complete nonredundant set to obtain effective Hessian matrix $\mathbf{f}^x_{sub}$. [b]Parameter "R" stands for bond stretching, and "α" is for angle bending. Unit of local mode force constant for bond stretchings and angles is mdyn/Å and mdyn×Å/rad^2 respectively.

coordinate parameters that are not included in the matrices of $\mathbf{B}'$ or $\mathbf{B}'_{sub}$ used for the extraction of $\mathbf{f}^x_{sub}$, and it is an evidence for the fact that the effective Hessian matrix $\mathbf{f}^x_{sub}$ retains the complete information in curvature of potential energy surface with regard to any possible internal coordinate within the subsystem.

4.5. Formaldehyde (CH_2O) in Carbon Nanotube (CNT). Recently, there has been an increasing number of studies focused on the design of CNTs as sensors for detecting formaldehyde.[62−64] For this purpose, a formaldehyde molecule was placed and stabilized within the model of a single-wall carbon nanotube (SWCNT) (Figure 7). Therefore, we check the vibrational modes of the formaldehyde molecule in the nanotube with GSVA.

In order to extract the effective Hessian matrix for the formaldehyde molecule, we choose a complete nonredundant set of parameters being composed of the three covalent bonds, two O−C−H angles, and one out-of-plane pyramidalization angle. Matrices $\mathbf{B}'$ and $\mathbf{B}'_{sub}$ used to recover $\mathbf{f}^x_{sub}$ have the dimensions of 6 × 252 and 6 × 12, respectively. The intrinsic fragmental vibrational frequencies are shown in Table 9. Comparing the fragmental vibrational frequencies for the formaldehyde molecule in the CNT with the normal vibrational frequencies of the reference formaldehyde in the gas phase, it is interesting that vibrations Nos. 1−3 have small frequency differences less than 4 cm^{-1}. Vibration No. 1 is dominated by the out-of-plane pyramidalization of the carbon atom with regard to the O−H−H plane. Vibration No. 2 is basically the in-plane rocking of two hydrogen atoms, while vibration No. 3

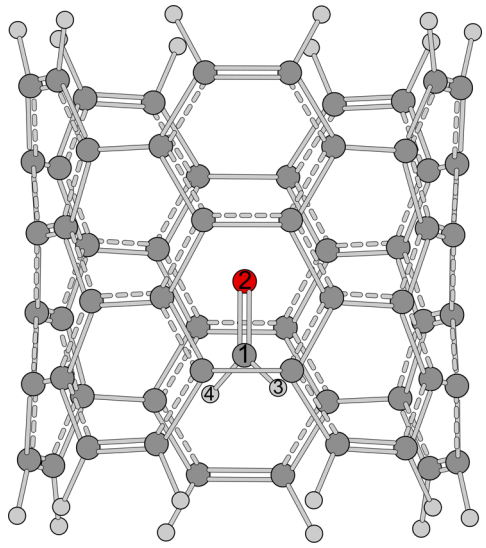

Figure 7. Structure of formaldehyde molecule contained in a carbon nanotube. Total number of atoms is 84.

Table 9. Comparison of Normal Mode Frequencies of Formaldehyde Molecule

No.	CH_2O in CNT (cm^{-1})	CH_2O in gas phase (cm^{-1})
1	1201	1201
2	1278	1275
3	1554	1555
4	1823	1847
5	2976	2897
6	3024	2954

is dominated by the in-plane scissoring of the H−C−H angle. Vibration No. 4 corresponds to the C═O bond stretching, and vibration No. 5 is associated with the symmetric C−H bond stretching mode. The largest deviation is found for vibration No. 6 which is dominated by the asymmetric stretching of two C−H bonds. This is a result of the confinement imposed on the formaldehyde molecule by the nanotube structure.

The validation of the intrinsic fragmental vibrational frequencies via the local mode analysis (Table 10) shows that the local mode properties for the subsystem based on the effective Hessian $\mathbf{f}^x_{sub}$ and full Hessian $\mathbf{f}^x$ are identical.

4.6. CH_2 and CH_3 Fragments in Propane. So far, we have applied GSVA to molecular subsystems under the perturbation of different chemical environments. However, we can also use GSVA to analyze the vibrations of fragments within a molecule and even compare the intrinsic fragmental vibrations of the same fragment in two different molecular systems.

As an example, we analyze the intrinsic fragmental vibrations in propane (Figure 8). By breaking all three C−C bonds, three fragments result, including two identical CH_3 fragments and one CH_2 fragment in the middle.

First, we applied GSVA to the CH_2 fragment. In analogy to H_2O, we chose two C−H bonds and the H−C−H angle as the internal coordinate set for constructing the effective Hessian matrix $\mathbf{f}^x_{sub}$. Therefore, the $\mathbf{B}'$ and $\mathbf{B}'_{sub}$ matrices have the dimensions of 3 × 33 and 3 × 9, respectively. The resulting fragmental vibrational modes are similar to the normal modes of H_2O. Vibration No. 1 is the H−C−H angle bending, and vibration No. 2 is the symmetric stretching of two C−H bonds.

DOI: 10.1021/acs.jctc.7b01171
J. Chem. Theory Comput. 2018, 14, 2558−2569

Table 10. Comparison of Local Mode Force Constants Based on Effective Hessian Matrix $\mathbf{f}^x_{sub}$ and Full Hessian Matrix $\mathbf{f}^x$ for Formaldehyde Molecule

No.[a]	q_n[b]	$k^a_{n,sub}$	k^a_n
1	R(1−2)	13.306	13.306
2	R(1−3)	4.924	4.924
3	R(1−4)	4.918	4.918
4	α(2−1−3)	1.109	1.109
5	α(2−1−4)	1.110	1.110
6	$\mathcal{P}$(1′-2−3−4)	3.496	3.496
7*	α(3−1−4)	0.833	0.833

[a]Parameter labeled with * indicates this internal coordinate is not used as part of the complete nonredundant set to obtain effective Hessian matrix $\mathbf{f}^x_{sub}$. [b]Parameter "R" stands for bond stretching, and "α" is for angle bending. "$\mathcal{P}$" is for out-of-plane pyramidalization, where the atom followed by a prime symbol moves with regard to the plane constructed by the other three atoms. Unit of local mode force constant for bond stretchings and angles is mdyn/Å and mdyn×Å/rad^2, respectively.

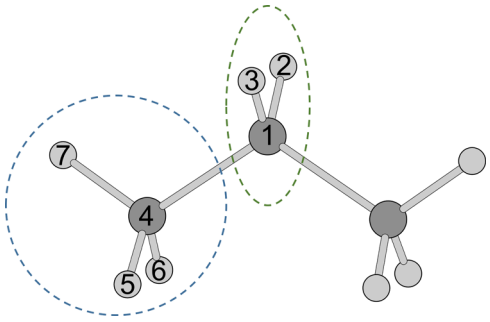

Figure 8. Structure of propane molecule in which the CH_2 and CH_3 fragments are highlighted with green and blue circles, respectively.

Vibration No. 3 is the asymmetric stretching of the same C−H bonds.

For the CH_3 fragment, we chose an analogy to the NH_3 molecule including three C−H bonds and three H−C−H angles as the complete nonredundant set to calculate its effective Hessian matrix $\mathbf{f}^x_{sub}$. Matrices $\mathbf{B}'$ and $\mathbf{B}'_{sub}$ in this regard are in the dimensions of 6 × 33 and 6 × 12, respectively. The mode characters of these six intrinsic fragmental vibrations are almost the same as the normal modes of ammonia due to their similar geometries. However, we need to note that the NH_3 molecule has C_{3v} symmetry, while the CH_3 fragment in propane has only C_s symmetry. Thus, vibrations Nos. 2−3 and Nos. 5−6 are no longer 2-fold degenerate, but they are still very close in pairs with regard to the frequency values.

Also, we take the intrinsic fragmental vibrations of CH_2 and CH_3 fragments in the methane (CH_4) molecule as the reference. In this way, the comparison of two intrinsic fragmental vibrational frequencies for the same CH_n fragment in propane and methane can be carried out as in Table 11.

The CH_3 fragments in methane molecule have 2-fold degenerate vibration pairs for vibrations Nos. 2−3 and Nos. 5−6 because the high symmetry is retained in both its geometry and corresponding effective Hessian matrix $\mathbf{f}^x_{sub}$. Noteworthy is that intrinsic fragmental vibrations associated with C−H stretching including Nos. 2 and 3 in the CH_2 fragment and Nos. 4−6 in the CH_3 fragment have larger frequency values in the reference methane molecule than in the propane molecule; this suggests that the C−H bonds in the methane molecule are

Table 11. Normal Mode Frequencies of Fragments in Propane Molecule and Reference Methane Molecule

No.	CH_2 in propane (cm^{-1})	CH_2 in methane (cm^{-1})	CH_3 in propane (cm^{-1})	CH_3 in methane (cm^{-1})
1	1622	1558	1543	1474
2	3178	3230	1602	1578
3	3209	3280	1605	1578
4	–	–	3174	3203
5	–	–	3235	3283
6	–	–	3242	3283

stronger than those in either the CH_2 or CH_3 fragments within propane.

Furthermore, the verification for the physical nature of the effective Hessian matrices $\mathbf{f}^x_{sub}$ for the CH_2 and CH_3 fragments in propane is shown in Table 12.

Table 12. Comparison of Local Mode Force Constants Based on Effective Hessian Matrix $\mathbf{f}^x_{sub}$ and Full Hessian Matrix $\mathbf{f}^x$ for Propane Molecule

No.[a]	q_n[b]	$k^a_{n,sub}$	k^a_n
A-1	R(1−2)	5.581	5.581
A-2	R(1−3)	5.581	5.581
A-3	α(2−1−3)	0.836	0.836
B-1	R(4−5)	5.649	5.649
B-2	R(4−6)	5.649	5.649
B-3	R(4−7)	5.684	5.684
B-4	α(5−4−6)	0.803	0.803
B-5	α(5−4−7)	0.801	0.801
B-6	α(6−4−7)	0.801	0.801

[a]In the "No." column, "A" denotes the CH_2 fragment, while "B" denotes the CH_3 fragment. [b]Parameter "R" stands for bond stretching, and "α" is for angle bending. Unit of local mode force constant for bond stretchings and angles is mdyn/Å and mdyn×Å/rad^2, respectively.

5. CONCLUSIONS

In this work, we have presented a new method to extract the intrinsic fragmental vibrations of a subsystem/fragment from an entire polyatomic molecular system. This method is different from its predecessors[2,3,6−11,14−16] which were designed or/and can be used for the same purpose in that our method is based on an effective Hessian matrix from which the curvature of the overall potential energy surface with regard to any internal coordinate parameter q_n within the subsystem is retained. The underlying solid physical foundation makes our method unique and able to characterize fragmental normal mode vibrations which are intrinsic to the subsystem/fragment in question. Therefore, our method is named the Generalized Subsystem Vibrational Analysis (GSVA), emphasizing its general applicability for any subsystem or fragment within a molecular system and concrete physical basis.

In the examples presented in this work, we compared the intrinsic fragmental vibrations of a subsystem with the normal vibrational modes of the isolated subsystem in gas phase to show the changes in the electronic structure caused by the presence of the environment. Although a more straightforward approach is to compare the corresponding properties of the local vibrational modes of the subsystem, the intrinsic fragmental vibrations can be regarded as a key intermediate

DOI: 10.1021/acs.jctc.7b01171
J. Chem. Theory Comput. 2018, 14, 2558−2569

linking the normal vibrational modes and the local vibrational modes in two aspects: (i) The intrinsic fragmental vibrations calculated by GSVA are in nature normal vibrational modes. (ii) These vibrations are based on the effective Hessian matrix taking the physical basis from Konkoli and Cremer's local vibrational modes,[31−34] namely, to retain the potential energy surface curvature of the whole system. In this regard, this work can be also considered as a theoretical extension to our previous work on the local vibrational modes.

A caveat is necessary when applying GSVA in theoretical chemical studies. The equilibrium geometry $\mathbf{R}_0$ for the entire molecular system including the subsystem to be studied is required by eq 1. The full Hessian matrix $\mathbf{f}^x$ describing the entire system is needed as one of the input data along with the geometry $\mathbf{R}_0$ and atomic masses $\mathbf{M}$. If one set of intrinsic fragmental vibrations is to be compared with another set of intrinsic fragmental vibrations for the same subsystem/fragment, we need to make sure that these two different molecular systems are being described with the same level of theory.

Concerning the implementation of GSVA into a computational chemistry package or as a standalone analysis program, three inputs are required to start with including the full Hessian matrix $\mathbf{f}^x$, geometry in Cartesian coordinates, and atomic masses. As the calculation of the effective Hessian matrix $\mathbf{f}^x_{sub}$ uses Wilson B matrices $\mathbf{B}'$ and $\mathbf{B}'_{sub}$ characterizing the complete nonredundant set of internal coordinates of the subsystem, a subroutine is expected for calculating Wilson B matrices for various internal coordinates, including bond length, bond angle, dihedral torsion angle, and so forth. Besides, the linear independence between rows of the B matrix should be checked and guaranteed in order for a complete and nonredundant set of $3n - k$ internal coordinates determining the geometry of the subsystem. Furthermore, a subroutine for solving the Wilson equation of vibrational spectroscopy is required to obtain normal vibrational modes.[65] By providing the effective Hessian matrix $\mathbf{f}^x_{sub}$, geometry, and atomic masses of the subsystem for the above subroutine, the normal mode vectors and frequencies can be obtained for the intrinsic fragmental vibrations. The computational cost of the whole calculation in GSVA is equivalent to doing the normal mode analysis for the entire system, and the most expensive part lies in the calculation of the Moore−Penrose inverse $(\mathbf{f}^x)^+$ of the full Hessian matrix.

This work provides a new and reliable theoretical tool for analyzing as well as comparing the molecular vibrations, and we anticipate our GSVA method to become a routine procedure in computational chemistry

AUTHOR INFORMATION

Corresponding Author

*E-mail: ekraka@smu.edu.

ORCID

Wenli Zou: 0000-0002-0747-2428

Dieter Cremer: 0000-0002-6213-5555

Elfi Kraka: 0000-0002-9658-5626

Notes

The authors declare no competing financial interest.

ACKNOWLEDGMENTS

Y.T. thanks Dr. Bernard Brooks for thought-provoking discussions during the 27th Austin Symposium on Molecular Structure and Dynamics at Dallas (ASMD@D This work was financially supported by the Natural Science Foundation (Grant 1464906). We thank SMU for providing computational resources.

DEDICATION

[⊥]This paper is in memoriam of Dr. Dieter Cremer.

REFERENCES

(1) Wilson, E. B.; Decius, J. C.; Cross, P. C. *Molecular Vibrations: The Theory of Infrared and Raman Vibrational Spectra*; Dover Publications: Mineola, NY, 2012.

(2) Head, J. D. Computation of Vibrational Frequencies for Adsorbates on Surfaces. *Int. J. Quantum Chem.* **1997**, *65*, 827−838.

(3) Li, H.; Jensen, J. H. Partial Hessian Vibrational Analysis: The Localization of the Molecular Vibrational Energy and Entropy. *Theor. Chem. Acc.* **2002**, *107*, 211−219.

(4) Besley, N. A.; Metcalf, K. A. Computation of the Amide I Band of Polypeptides and Proteins using a Partial Hessian Approach. *J. Chem. Phys.* **2007**, *126*, 035101.

(5) Besley, N. A.; Bryan, J. A. Partial Hessian Vibrational Analysis of Organic Molecules Adsorbed on Si(100). *J. Phys. Chem. C* **2008**, *112*, 4308−4314.

(6) Ghysels, A.; Van Neck, D.; Van Speybroeck, V.; Verstraelen, T.; Waroquier, M. Vibrational Modes in Partially Optimized Molecular Systems. *J. Chem. Phys.* **2007**, *126*, 224102.

(7) Ghysels, A.; Van Neck, D.; Waroquier, M. Cartesian Formulation of the Mobile Block Hessian Approach to Vibrational Analysis in Partially Optimized Systems. *J. Chem. Phys.* **2007**, *127*, 164108.

(8) Ghysels, A.; Van Neck, D.; Brooks, B. R.; Van Speybroeck, V.; Waroquier, M. Normal Modes for Large Molecules with Arbitrary Link Constraints in the Mobile Block Hessian Approach. *J. Chem. Phys.* **2009**, *130*, 084107.

(9) Ghysels, A.; Van Speybroeck, V.; Pauwels, E.; Van Neck, D.; Brooks, B. R.; Waroquier, M. Mobile Block Hessian Approach with Adjoined Blocks: An Efficient Approach for the Calculation of Frequencies in Macromolecules. *J. Chem. Theory Comput.* **2009**, *5*, 1203−1215.

(10) Ghysels, A.; Van Speybroeck, V.; Verstraelen, T.; Van Neck, D.; Waroquier, M. Calculating Reaction Rates with Partial Hessians: Validation of the Mobile Block Hessian Approach. *J. Chem. Theory Comput.* **2008**, *4*, 614−625.

(11) Woodcock, H. L.; Zheng, W.; Ghysels, A.; Shao, Y.; Kong, J.; Brooks, B. R. Vibrational Subsystem Analysis: A Method for Probing Free Energies and Correlations in the Harmonic Limit. *J. Chem. Phys.* **2008**, *129*, 214109.

(12) Hafner, J.; Zheng, W. Approximate Normal Mode Analysis Based on Vibrational Subsystem Analysis with High Accuracy and Efficiency. *J. Chem. Phys.* **2009**, *130*, 194111.

(13) Ghysels, A.; Miller, B. T.; Pickard, F. C.; Brooks, B. R. Comparing Normal Modes Across Different Models and Scales: Hessian Reduction versus Coarse-Graining. *J. Comput. Chem.* **2012**, *33*, 2250−2275.

(14) Ghysels, A.; Van Speybroeck, V.; Pauwels, E.; Catak, S.; Brooks, B. R.; Van Neck, D.; Waroquier, M. Comparative Study of Various Normal Mode Analysis Techniques Based on Partial Hessians. *J. Comput. Chem.* **2010**, *31*, 994−1007.

(15) Jacob, C. R.; Reiher, M. Localizing Normal Modes in Large Molecules. *J. Chem. Phys.* **2009**, *130*, 084106.

(16) Huix-Rotllant, M.; Ferré, N. An Effective Procedure for Analyzing Molecular Vibrations in Terms of Local Fragment Modes. *J. Chem. Theory Comput.* **2016**, *12*, 4768−4777.

(17) Foster, J. M.; Boys, S. F. Canonical Configurational Interaction Procedure. *Rev. Mod. Phys.* **1960**, *32*, 300−302.

(18) Edmiston, C.; Ruedenberg, K. Localized Atomic and Molecular Orbitals. *Rev. Mod. Phys.* **1963**, *35*, 457−464.

(19) Pipek, J.; Mezey, P. G. A Fast Intrinsic Localization Procedure Applicable for ab initio and Semiempirical Linear Combination of Atomic Orbital Wave Functions. *J. Chem. Phys.* **1989**, *90*, 4916−4926.

DOI: 10.1021/acs.jctc.7b01171
J. Chem. Theory Comput. 2018, 14, 2558−2569

(20) Weinhold, F.; Landis, C. R. Natural Bond Orbitals and Extensions of Localized Bonding Concepts. *Chem. Educ. Res. Pract.* **2001**, *2*, 91−104.
(21) Høyvik, I.-M.; Jansik, B.; Jørgensen, P. Orbital Localization using Fourth Central Moment Minimization. *J. Chem. Phys.* **2012**, *137*, 224114.
(22) Mulliken, R. S. Electronic Population Analysis on LCAO−MO Molecular Wave Functions. I. *J. Chem. Phys.* **1955**, *23*, 1833−1840.
(23) Hirshfeld, F. L. Bonded-Atom Fragments for Describing Molecular Charge Densities. *Theor. Chem. Acc.* **1977**, *44*, 129−138.
(24) Foster, J. P.; Weinhold, F. Natural Hybrid Orbitals. *J. Am. Chem. Soc.* **1980**, *102*, 7211−7218.
(25) Chirlian, L. E.; Francl, M. M. Atomic Charges Derived from Electrostatic Potentials: A Detailed Study. *J. Comput. Chem.* **1987**, *8*, 894−905.
(26) Breneman, C. M.; Wiberg, K. B. Determining Atom-Centered Monopoles from Molecular Electrostatic Potentials. The Need for High Sampling Density in Formamide Conformational Analysis. *J. Comput. Chem.* **1990**, *11*, 361−373.
(27) Besler, B. H.; Merz, K. M.; Kollman, P. A. Atomic Charges Derived from Semiempirical Methods. *J. Comput. Chem.* **1990**, *11*, 431−439.
(28) Bader, R. F. W. A Quantum Theory of Molecular Structure and its Applications. *Chem. Rev.* **1991**, *91*, 893−928.
(29) Bader, R. F. W. *Atoms in Molecules: A Quantum Theory*; Clarendon Press: Oxford, UK, 1994.
(30) Zou, W.; Kalescky, R.; Kraka, E.; Cremer, D. Relating Normal Vibrational Modes to Local Vibrational Modes with the Help of an Adiabatic Connection Scheme. *J. Chem. Phys.* **2012**, *137*, 084114.
(31) Konkoli, Z.; Cremer, D. A New Way of Analyzing Vibrational Spectra. I. Derivation of Adiabatic Internal Modes. *Int. J. Quantum Chem.* **1998**, *67*, 1−9.
(32) Konkoli, Z.; Larsson, J. A.; Cremer, D. A New Way of Analyzing Vibrational Spectra. II. Comparison of Internal Mode Frequencies. *Int. J. Quantum Chem.* **1998**, *67*, 11−27.
(33) Konkoli, Z.; Cremer, D. A New Way of Analyzing Vibrational Spectra. III. Characterization of Normal Vibrational Modes in terms of Internal Vibrational Modes. *Int. J. Quantum Chem.* **1998**, *67*, 29−40.
(34) Konkoli, Z.; Larsson, J. A.; Cremer, D. A New Way of Analyzing Vibrational Spectra. IV. Application and Testing of Adiabatic Modes Within the Concept of the Characterization of Normal Modes. *Int. J. Quantum Chem.* **1998**, *67*, 41−55.
(35) Zou, W.; Cremer, D. Properties of Local Vibrational Modes: The Infrared Intensity. *Theor. Chem. Acc.* **2014**, *133*, 1451.
(36) Kalescky, R.; Zou, W.; Kraka, E.; Cremer, D. Local vibrational modes of the water dimer - Comparison of theory and experiment. *Chem. Phys. Lett.* **2012**, *554*, 243−247.
(37) Freindorf, M.; Kraka, E.; Cremer, D. A Comprehensive Analysis of Hydrogen Bond Interactions Based on Local Vibrational Modes. *Int. J. Quantum Chem.* **2012**, *112*, 3174−3187.
(38) Zou, W.; Cremer, D. C_2 in a Box: Determining its Intrinsic Bond Strength for the $X^1\Sigma_g^+$ Ground State. *Chem. - Eur. J.* **2016**, *22*, 4087−4099.
(39) Kalescky, R.; Kraka, E.; Cremer, D. Identification of the Strongest Bonds in Chemistry. *J. Phys. Chem. A* **2013**, *117*, 8981−8995.
(40) Tao, Y.; Zou, W.; Jia, J.; Li, W.; Cremer, D. Different Ways of Hydrogen Bonding in Water - Why Does Warm Water Freeze Faster than Cold Water? *J. Chem. Theory Comput.* **2017**, *13*, 55−76.
(41) Cremer, D.; Kraka, E. Generalization of the Tolman Electronic Parameter: the Metal-ligand Electronic Parameter and the Intrinsic Strength of the Metal-ligand Bond. *Dalton Trans.* **2017**, *46*, 8323−8338.
(42) Tao, Y.; Zou, W.; Kraka, E. Strengthening of Hydrogen Bonding with the Push-pull Effect. *Chem. Phys. Lett.* **2017**, *685*, 251−258.
(43) Tao, Y.; Zou, W.; Cremer, D.; Kraka, E. Characterizing Chemical Similarity With Vibrational Spectroscopy: New Insights Into the Substituent Effects in Mono-Substituted Benzenes. *J. Phys. Chem. A* **2017**, *121*, 8086−8096.
(44) Tao, Y.; Zou, W.; Cremer, D.; Kraka, E. Correlating the Vibrational Spectra of Structurally Related Molecules: A Spectroscopic Measure of Similarity. *J. Comput. Chem.* **2018**, *39*, 293−306.
(45) Wilson, E. B. A Method of Obtaining the Expanded Secular Equation for the Vibration Frequencies of a Molecule. *J. Chem. Phys.* **1939**, *7*, 1047−1052.
(46) Brandhorst, K.; Grunenberg, J. Efficient Computation of Compliance Matrices in Redundant Internal Coordinates from Cartesian Hessians for Nonstationary Points. *J. Chem. Phys.* **2010**, *132*, 184101.
(47) Frisch, M. J.; Trucks, G. W.; Schlegel, H. B.; Scuseria, G. E.; Robb, M. A.; Cheeseman, J. R.; Scalmani, G.; Barone, V.; Mennucci, B.; Petersson, G. A.; Nakatsuji, H.; Caricato, M.; Li, X.; Hratchian, H. P.; Izmaylov, A. F.; Bloino, J.; Zheng, G.; Sonnenberg, J. L.; Hada, M.; Ehara, M.; Toyota, K.; Fukuda, R.; Hasegawa, J.; Ishida, M.; Nakajima, T.; Honda, Y.; Kitao, O.; Nakai, H.; Vreven, T.; Montgomery, J. A., Jr.; Peralta, P. E.; Ogliaro, F.; Bearpark, M.; Heyd, J. J.; Brothers, E.; Kudin, K. N.; Staroverov, V. N.; Kobayashi, R.; Normand, J.; Raghavachari, K.; Rendell, A.; Burant, J. C.; Iyengar, S. S.; Tomasi, J.; Cossi, M.; Rega, N.; Millam, N. J.; Klene, M.; Knox, J. E.; Cross, J. B.; Bakken, V.; Adamo, C.; Jaramillo, J.; Gomperts, R.; Stratmann, R. E.; Yazyev, O.; Austin, A. J.; Cammi, R.; Pomelli, C.; Ochterski, J. W.; Martin, R. L.; Morokuma, K.; Zakrzewski, V. G.; Voth, G. A.; Salvador, P.; Dannenberg, J. J.; Dapprich, S.; Daniels, A. D.; Farkas, Ö.; Ortiz, J. V.; Cioslowski, J.; Fox, D. J. *Gaussian 09*, revision E.01 ; Gaussian, Inc.: Wallingford, CT, 2009.
(48) Chai, J.-D.; Head-Gordon, M. Long-Range Corrected Hybrid Density Functionals with Damped Atom-atom Dispersion Corrections. *Phys. Chem. Chem. Phys.* **2008**, *10*, 6615−6620.
(49) Ditchfield, R.; Hehre, W. J.; Pople, J. A. Self-Consistent Molecular-Orbital Methods. IX. An Extended Gaussian-Type Basis for Molecular-Orbital Studies of Organic Molecules. *J. Chem. Phys.* **1971**, *54*, 724−728.
(50) Hariharan, P. C.; Pople, J. A. The Influence of Polarization Functions on Molecular Orbital Hydrogenation Energies. *Theor. Chem. Acc.* **1973**, *28*, 213−222.
(51) Clark, T.; Chandrasekhar, J.; Spitznagel, G. W.; Schleyer, P. V. R. Efficient Diffuse Function-augmented Basis Sets for Anion Calculations. III. The 3-21+G Basis Set for First-Row Elements, Li-F. *J. Comput. Chem.* **1983**, *4*, 294−301.
(52) Becke, A. D. Density-Functional Thermochemistry. III. The Role of Exact Exchange. *J. Chem. Phys.* **1993**, *98*, 5648−5652.
(53) Lee, C.; Yang, W.; Parr, R. G. Development of the Colle-Salvetti Correlation-Energy Formula into a Functional of the Electron Density. *Phys. Rev. B: Condens. Matter Mater. Phys.* **1988**, *37*, 785−789.
(54) Vosko, S. H.; Wilk, L.; Nusair, M. Accurate Spin-Dependent Electron Liquid Correlation Energies for Local Spin Density Calculations: A Critical Analysis. *Can. J. Phys.* **1980**, *58*, 1200−1211.
(55) Stephens, P. J.; Devlin, F. J.; Chabalowski, C. F.; Frisch, M. J. Ab Initio Calculation of Vibrational Absorption and Circular Dichroism Spectra Using Density Functional Force Fields. *J. Phys. Chem.* **1994**, *98*, 11623−11627.
(56) Zhao, Y.; Truhlar, D. G. The M06 Suite of Density Functionals for Main Group Thermochemistry, Thermochemical Kinetics, Noncovalent Interactions, Excited States, and Transition Elements: Two New Functionals and Systematic Testing of Four M06-class Functionals and 12 Other Functionals. *Theor. Chem. Acc.* **2008**, *120*, 215−241.
(57) Grimme, S.; Antony, J.; Ehrlich, S.; Krieg, H. A Consistent and Accurate ab initio Parametrization of Density Functional Dispersion Correction (DFT-D) for the 94 Elements H-Pu. *J. Chem. Phys.* **2010**, *132*, 154104.
(58) Grimme, S.; Ehrlich, S.; Goerigk, L. Effect of the Damping Function in Dispersion Corrected Density Functional Theory. *J. Comput. Chem.* **2011**, *32*, 1456−1465.
(59) Roothaan, C. C. J. New Developments in Molecular Orbital Theory. *Rev. Mod. Phys.* **1951**, *23*, 69−89.
(60) Kraka, E.; Zou, W.; Filatov, M.; Tao, Y.; Grafenstein, J.; Izotov, D.; Gauss, J.; He, Y.; Wu, A.; Konkoli, Z.; Polo, V.; Olsson, L.; He, Z.;

DOI: 10.1021/acs.jctc.7b01171
J. Chem. Theory Comput. 2018, 14, 2558−2569

Cremer, D. COLOGNE2017, 2017; http://www.smu.edu/catco (accessed April 2018).
(61) Morosin, B.; Assink, R.; Dunn, R.; Massis, T.; Schirber, J.; Kwei, G. Methane-intercalated C60: Preparation, Orientational Ordering, and Structure. *Phys. Rev. B: Condens. Matter Mater. Phys.* **1997**, *56*, 13611−13614.
(62) Lu, Y.; Meyyappan, M.; Li, J. A Carbon-Nanotube-based Sensor Array for Formaldehyde Detection. *Nanotechnology* **2011**, *22*, 055502.
(63) Kim, J. Y.; Lee, J.; Hong, S.; Chung, T. D. Formaldehyde Gas Sensing Chip based on Single-Walled Carbon Nanotubes and Thin Water Layer. *Chem. Commun.* **2011**, *47*, 2892−2894.
(64) Tang, R.; Shi, Y.; Hou, Z.; Wei, L. Carbon Nanotube-Based Chemiresistive Sensors. *Sensors* **2017**, *17*, 882.
(65) Ochterski, J. *White Paper: Vibrational analysis in Gaussian*; Gaussian, 1999.

DOI: 10.1021/acs.jctc.7b01171
J. Chem. Theory Comput. 2018, 14, 2558−2569